Title: Regional Source-type Discrimination Using Nonlinear Alignment Algorithms

Authors: Marlon D. Ramos, Rigobert Tibi, Christopher J. Young, Erica L. Emry

Author Affiliation(s): Sandia National Laboratories

Corresponding Author Contact Information:
Email: mdramos@sandia.gov
Address: Sandia National Laboratories / Marlon Ramos, Mail Stop 0404 / PO Box 5800 / Albuquerque, NM 87185

Abstract

The discrimination problem in seismology aims to accurately classify different underground source types based on local, regional and/or teleseismic observations of ground motion. Typical discriminant approaches are rooted in fundamental, physics-based differences in radiation pattern or wave excitation, which can be frequency dependent and may not make use of the full waveform. In this paper, we explore whether phase and amplitude distances derived from dynamic time warping (DTW) and elastic shape analysis (ESA) can inform event discrimination. We demonstrate the ability to distinguish underground point-sources using synthetic waveforms calculated for a 1-D Earth model and various source mechanisms. We then apply the method to recorded data from events in the Korean Peninsula, which includes declared nuclear explosions, a collapse event, and naturally occurring earthquakes. Phase and amplitude distances derived from DTW and ESA are then used to classify the event types via dendrogram and k-nearest neighbor clustering analyses. Using information from the full waveform, we show how different underground sources can be distinguished at regional distances. We highlight the potential of these nonlinear alignment algorithms for discrimination and comment on ways we can extend the framework presented here.

Introduction

Source type discrimination is needed to classify events for nuclear treaty or seismic hazard monitoring purposes. Traditional discriminants exploit physics-based intuition that the radiation pattern of double-couple sources (e.g., earthquakes) should be fundamentally different from explosion-like sources (e.g., chemical/nuclear tests, mining blasts). This is due to the difference in the repartition of energy release that exists between shear slip and a pressure pulse acting on the rock (Ben-Menahem and Singh, 1981). Approaches to discrimination between seismic events include moment tensor inversion (e.g., Alvizuri and Tape, 2018; Pasyanos and Chiang, 2022), body to surface-wave magnitude ratios (M_s:m_b, e.g., Stevens and Day, 1985), spectral amplitude ratios (e.g., Tibi, 2021) and recently, machine learning methods (e.g., Kong et al., 2022; Maguire et al., 2024; Linville et al., 2019). Many of these established discrimination methods are successful because specific diagnostic parts of the seismic waveform can be analyzed in the time or frequency domain using narrow passbands, or, in the case of moment tensor inversion, the full moment tensor can be estimated, and the proportion of double-couple and non-double couple components determined. Limitations to the above methods may include difficulty to achieve satisfactory phase separation at local distances (e.g., Tibi et al., 2023), constraints on event size (i.e., total moment release) or in the case of machine learning, analysts may not have enough large, labeled datasets to draw from for a given region of interest.

Nonlinear dynamic programming techniques, broadly referred to as dynamic time warping (DTW), have been used to determine what temporal shifts are necessary to optimally align time series (Anderson and Gaby, 1983; Kumar et al., 2022; Müller, 2021). DTW has been applied in seismic exploration (Hale, 2013), ambient-noise interferometry (Mikesell et al., 2015; Yuan et al., 2021) and linear seismic inversion problems (Tan and Langston, 2022). DTW algorithms capture phase variability quite well but may not be as robust to amplitude variability (Müller et al., 2021). This is a concern for seismic event monitoring and especially in the context of signal window selection, which can contain both body and surface waves with markedly different amplitudes. A novel representation of functional data that addresses both phase and amplitude variability within a time series is elastic shape analysis of curves (ESA; Tucker et al., 2013). The ESA method aligns signals to one another after applying a square root slope function (SRSF; Joshi et al., 2007; Srivastava et al., 2011). The SRSF is a distance-preserving transformation between metric spaces (isometry) and yields a proper distance in either phase or amplitude space. Our hypothesis is that two signals sharing the same source mechanism and similar Green's functions will have a lower phase or amplitude distance whereas signals that do not will have correspondingly higher distances. Moreover, nonlinear alignment methods are not constrained by phase separation, narrow time windows, or event size.

This manuscript explores whether nonlinear time series alignment algorithms might assist event type discrimination. First, we set up a simple synthetic test relevant to regional distance monitoring to see if DTW and ESA can distinguish double couple from non-double couple (e.g., explosive) signals. Because the synthetic test supports this hypothesis, we then analyze a real seismic dataset of earthquake, explosion, and collapse events in the Democratic People's Republic of Korea (DPRK) and apply hierarchical clustering and k-nearest neighbor (knn) analysis to the DTW and ESA distances to see whether the method works to distinguish event types using a real discrimination scenario. We compare the DTW and ESA methods, contrast our approach to existing discriminants, and discuss recommendations to extend this preliminary analysis.

Methodology

Dynamic Time Warping

DTW estimates time shifts between signals to estimate geophysical parameters and can overcome strong cycle-skipping even in the presence of low signal to noise-ratio (SNR), which is an advantage over windowed cross-correlation and linear trace stretching methods that may estimate incorrect lag times (Mikesell et al., 2015). However, to optimally align signals, unrealistically large dilation of the original time series can occur and strategies to constrain the dynamic programming algorithm (i.e., global or local constraints on the permissible warping function) to reasonable dilation values are not always easy to set a-priori. Despite these choices, DTW allows one to calculate a non-Euclidian distance metric that gives a measure of how much warping was needed for optimal alignment, the DTW distance (DTW_{dist}), defined below as,

$$DTW_{dist}(f_1, f_2) = \min\{w_p(f_1, f_2)\} \tag{1}$$

where w_p is the warping path that aligns $f_1(t)$ and $f_2(t)$ after an accumulated distance matrix is computed (Müller, 2021).

Elastic Shape Analysis

ESA separates amplitude and phase information uniquely by first computing the SRSF, $q(t)$,

$$q(t) = sign(f(\dot{t}))\sqrt{|f(\dot{t})|} \tag{2}$$

where $q(t)$ is the transformed signal and $f(\dot{t})$ is the first derivative of the original signal with respect to time (Srivistava et al., 2011). The amplitude distance (D_y) between two functions $f_1(t)$ and $f_2(t)$ is defined as,

$$D_y(f_1, f_2) = inf_{\gamma \in \Gamma} \parallel q_1 - (q_2 \circ \gamma)\sqrt{\dot{\gamma}} \parallel \tag{3}$$

where q_1 and q_2 are the SRSF of $f_1(t)$ and $f_2(t)$, respectively, and γ is the warping function that best aligns them. The double-bars "|| ||" denote the L2-norm and Γ represents the complete set of invertible functions that map a smooth surface to each another such that both the function and its inverse are well defined over [0,1]. The phase distance (D_x) is then defined as the distance between warping functions according to,

$$D_x(\gamma_1, \gamma_2) = d_\psi(\psi_1, \psi_2) \equiv \cos^{-1}(\int_0^1 \psi_1(t)\psi_2(t)\, dt) \tag{4}$$

where ψ(t) represents a mapping of the warping function to Hilbert space ($\mathcal{H}$) and D_x is thus the arc-length between the corresponding SRSF on a $\mathcal{H}$ unit sphere. The theory behind elastic distances is rich, and we refer the interested reader to Wu and Srivastava (2011), Srivastava et al., (2011) or Tucker et al., (2013) for the in-depth, mathematical underpinnings of D_x and D_y. The important properties of ESA that distinguish this method from typical DTW algorithms are: 1) D_y and D_x are independent of one another, 2) the SRSF transformation guarantees a mathematically proper distance, and 3) the distances are invariant to warping order.

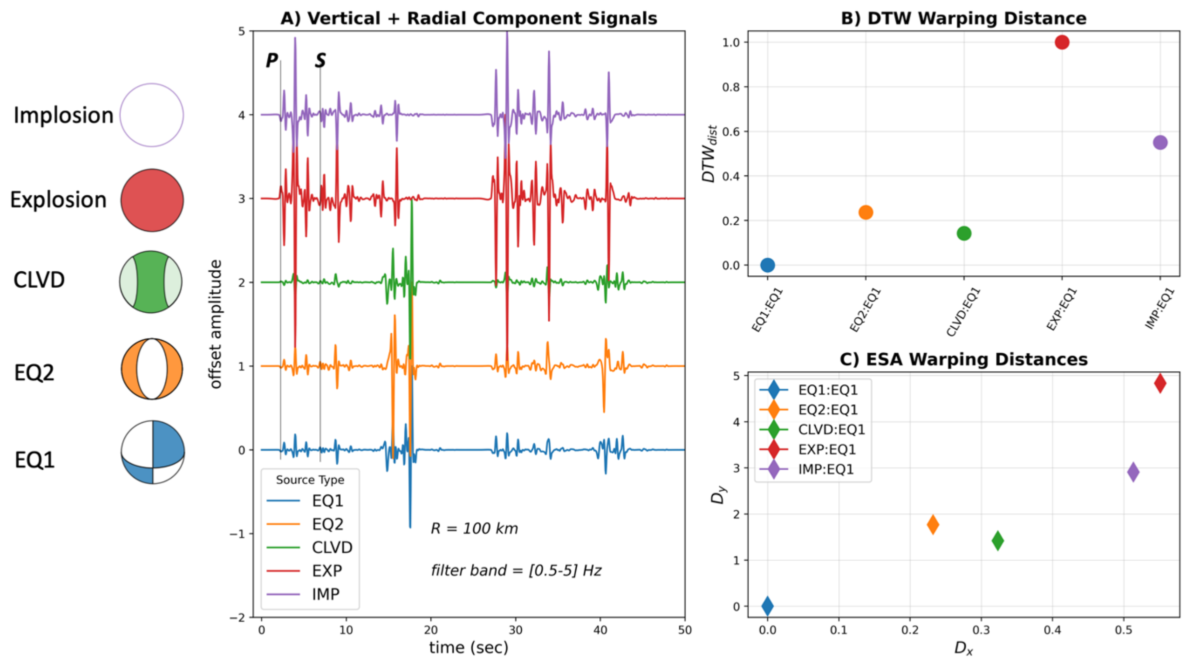

Figure 1. A) Concatenated vertical (Z) and radial (R) component synthetics calculated for the Ford et al. (2009) velocity model recorded at a source-receiver distance of 100 km assuming an azimuth of 30 degrees and hypocenter depth of 1 km. Source mechanisms range from purely double-couple (bottom) to implosive (top) sources. The waveforms are normalized to their respective maximum amplitude and distinct phase arrival times are denoted by thin gray lines on Z components. Direct P and S are labeled. B) Dynamic time warping distance (DTW_{dist}) between each waveform pair relative to EQ1, normalized by the largest DTW_{dist}. C) Elastic phase (D_x) and amplitude (D_y) distances for each warping pair (unnormalized). Legend in C applies to subfigures B and C.

Synthetic Data Experiment

We generate near-regional synthetic seismic waveforms using a 1-D velocity model developed for the DPRK to conceptually represent a realistic monitoring scenario where closely spaced and different underground sources are recorded by a single seismic station (Ford et al., 2009; Figure 1). We use a wave-number integration algorithm (Herrmann, 2013) to calculate synthetics for double-couple, compensated linear vector dipole (CLVD), pure explosion, and implosion point-sources recorded at 100 km distance (Figure 1A). We calculate only the down-going Green's function components to suppress strong free-surface effects on the waveform. This lets us simplify and focus our analysis on waveform differences due to source mechanism alone. We filter the 40-samples-per-second synthetic waveforms between 0.5 to 5 Hz (Tibi, 2021) and normalize each trace by its respective maximum amplitude prior to alignment. We also concatenate the vertical (Z) and radial (R) components into a composite time series before warping and alignment to mimic practice in signal detection. Note that for a pure isotropic explosion source, there is no tangential (T) motion generated and thus that component is not considered in the synthetic analysis because discrimination would be trivial.

At 100-km source-receiver distance, we select a double-couple earthquake waveform as the main signal to align to (EQ1, Figure 1A). Each waveform has a P-wave arrival near 15 seconds after the respective event origin time, but to highlight phase arrivals of interest, we cut the waveforms from 15 to 40 seconds for both R and Z components. We warp every signal to EQ1 and calculate DTW_{dist}, D_x and D_y (Figure 1B, C). We observe that for both DTW and ESA, the distance between EQ1 and itself is zero (expected) and the explosion and implosion events have greater phase and amplitude distances than alignment to the earthquake or CLVD events. Because the Green's function is the same for each waveform, this synthetic experiment suggests that differences due to source mechanism can be inferred via phase or amplitude distance information from DTW and ESA between the full waveforms. It is important to keep in mind that the source mechanism and velocity model are kept simple to illustrate how warping distances can distinguish underground event types.

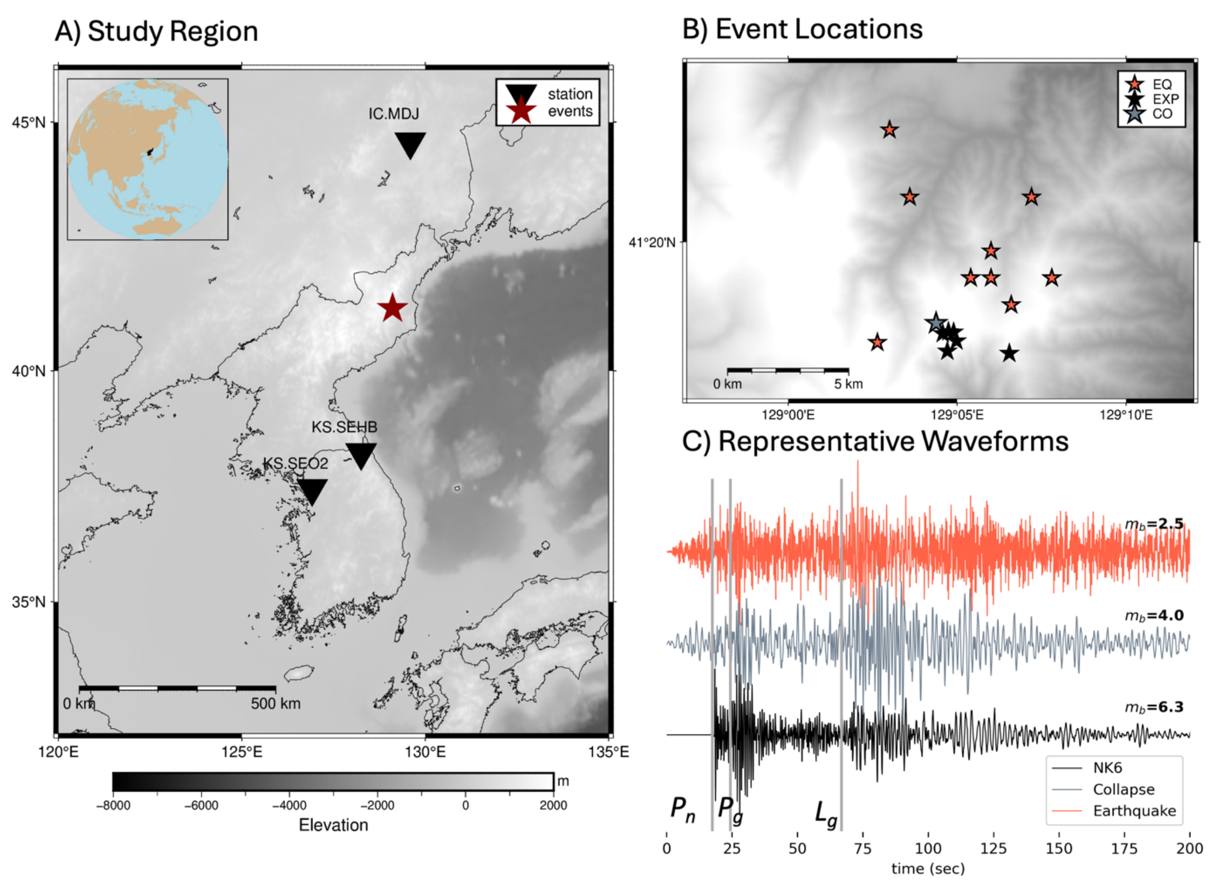

Figure 2. A) Map of DPRK and surrounding region showing seismic stations used in the cluster analysis. Average epicenter of the NK1 - NK6 tests, collapse event, and naturally occurring earthquakes is denoted by the red star. B) Event epicenters near Mount Mantap. Several earthquakes (EQ) are < 1 km distance apart and thus may be plotted on top of one another. C) Example vertical-component waveforms of an explosion, collapse and earthquake event recorded at station MDJ (network IC). National Earthquake Information Center body-wave magnitudes (m_b) tabulated

on the righthand side of the plot. Filter passband is between 0.5 – 5 Hz. A group velocity of 3.6 km/s is assumed to estimate the L_g arrival whereas the PREM earth model is used to calculate P_n and P_g arrival times.

Real Data Analysis: DPRK

For the observational dataset, we use waveforms analyzed in Tibi (2021). This dataset contains six declared explosions, fifteen nearby naturally occurring earthquakes and one collapse event following the 2017 declared North Korean nuclear test (Figure 2). All events are within a 10-km epicentral distance of one another. Three regional broadband stations are selected from the IC, IU, and KS seismic networks. We download waveforms up to 15 minutes after the respective origin time of the events from the Incorporated Research Institutions for Seismology (IRIS) database to ensure P_n, P_g, and L_g phases are captured, and we filter signals below 10 Hz. Due to different station start and end times, not all events are recorded; also, stations with non-emergent phases are excluded from analysis.

Regional seismic stations recorded the declared 2006 (NK1), 2009 (NK2), 2013 (NK3), 2016 (NK4, NK5) and 2017 (NK6) DPRK nuclear tests, one collapse event following NK6, and explosion-induced aftershocks or isolated, natural seismicity (Figure 2B). We use a subset of the stations used in Tibi (2021) to assess DTW and ESA performance on each event pair combination in this set of closely spaced events (Figure 2B). For any station, the signal time window spans five seconds before theoretically expected P_n and ~40 seconds after the L_g arrival (Figure 2C).

We select data from a single station (MDJ, vertical component) to demonstrate how nonlinear alignment between dissimilar signals may result in larger amplitude (D_y) or phase (D_x, DTW_{dist}) distance. We select two earthquakes (EQ1 and EQ2; Figure 3A), an explosion from the 2006 declared nuclear test (NK1; Figure 3A) and the collapse event following the largest declared nuclear test for this exercise (CO; Figure 3A). P_n, P_g and L_g phases are readily identifiable on all waveforms. Because the explosions have different yields and are not exactly co-located (Myers et al., 2018), nonlinear warping must address differences from both the source mechanism and Green's functions. Selecting EQ1 has the main signal to align to, we show how the waveforms must be warped to accomplish this using DTW (Figure 3B) and ESA (Figure 3C) approaches. The warping functions (and the phase or amplitude distances that are computed after alignment) are given in Figure 3D and 3E. We note that in all cases, if two dissimilar event type waveforms are aligned to one another (e.g., an earthquake to an explosion), then a *larger* D_y, D_x and DTW_{dist} is indeed observed and the warping function deviates significantly from the one-to-one diagonal line, which would be the warping path between two identical signals (Figure 3D, 3E). We also calculate the cross-correlation coefficient (CC) before and after alignment and note that whereas DTW and ESA both increase CC (an exception being between EQ1 and EQ2 using ESA, but the differences is < 0.1), DTW (with no constraints on the warping path) can increase CC by as much as 0.7 units. Such stellar alignment, however, comes at the cost of appreciable waveform stretching (i.e., Figure 3B).

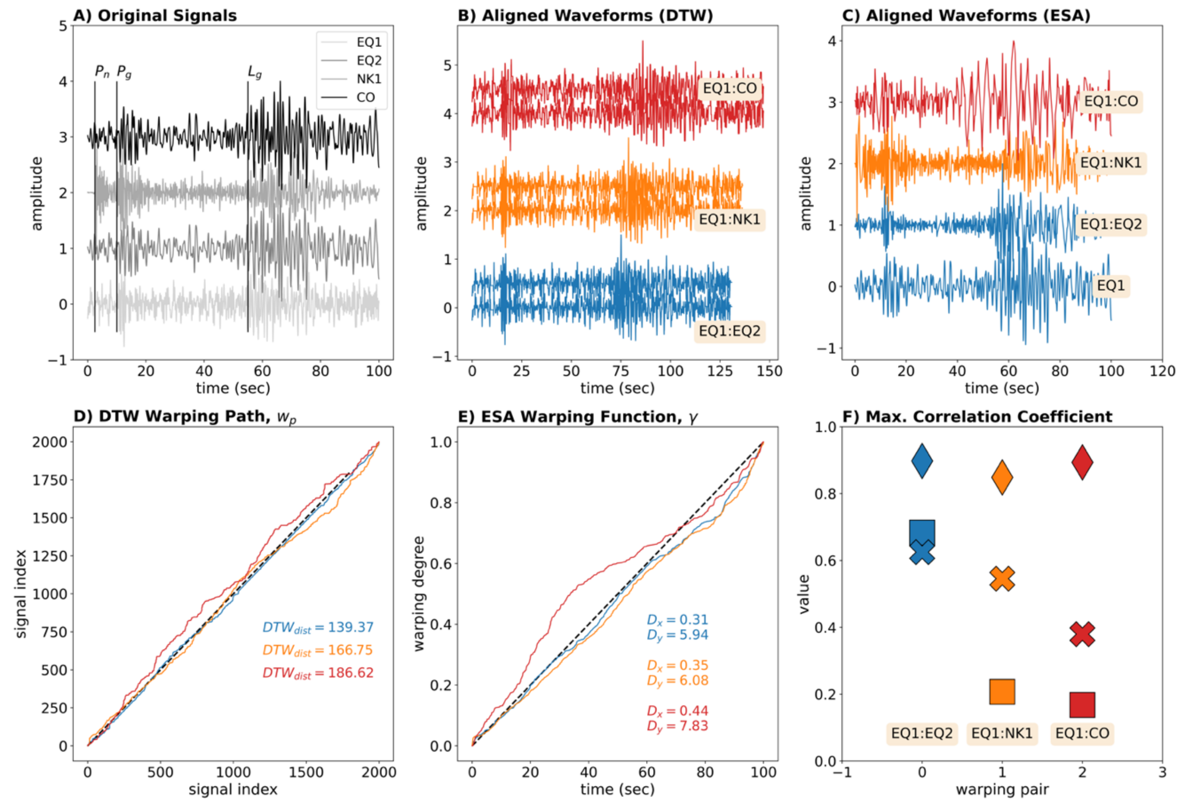

Figure 3. Demonstration of how nonlinear warping algorithms may be able to distinguish underground event types. A) Vertical component waveforms recorded at station MDJ filtered between 0.5 and 3 Hz. EQ1 and EQ2 are m_b 2.5 and 3.4, respectively. NK1 = declared nuclear explosion test on 2006/10/09 (m_b 4.3) and CO = collapse event following declared nuclear explosion NK6 on 2017/09/03 (m_b 4.0) B) Waveforms of each event warped to match EQ1 using dynamic time warping (DTW). C) Waveforms of each event warped to match EQ1 using elastic shape analysis (ESA). D) The warping paths between each signal pair in panel B. The dynamic time warping distances (DTW_{dist}) are tabulated in the lower right corner. E) The warping function through time for each signal pair in C. Here, both phase (D_x) and amplitude (D_y) distances are given in the lower right corner. For both D) and E) the diagonal dashed line signifies what the warping path would be if no distortion between signals was needed for alignment. F) The cross-correlation coefficient before (squares), after DTW (diamonds) and after ESA (crosses) alignment.

We next compute DTW and ESA for each pair across all stations and apply hierarchical clustering analysis to the DTW and ESA distances obtained. We show the analysis for MDJ in Figure 4. We also report CC between each pair to see where a particular distance metric may align with empirical signal similarity (Figure 4D). We calculate condensed matrix representations of D_x, D_y, and DTW_{dist} and show the results graphically using a dendrogram (Figure 4E, F). We observe more structure in the D_y and DTW_{dist} matrices, based off a qualitative comparison to the cross-correlation matrix. When an earthquake is warped to an explosion (or vice versa), we generally observe a higher phase or amplitude distance (Figure 4A, B) and a lower CC score (Figure 4C). In contrast, the collapse event is not as easy to discern without additional information.

To assess whether we can achieve better classification between earthquake, explosion and collapse events using both phase and amplitude information, we form a simple linear combination of D_x and D_y following Tucker et al., (2014), using a weighting coefficient, τ. Since D_y appears to have more structure than D_x, we weight D_y more in the below formulation,

$$D_\tau = \tau D_y + (1 - D_x)\tau \qquad (5)$$

To optimize the weighting coefficient τ, we randomly set aside 50% of the signals as training data (Tucker et al., 2014) and employ a Leave-One-Out (LOO) cross-validated knn classifier for varying τ levels ($0 \leq \tau \leq 1$ in an increment of 0.1) in expression (5). We set the value of knn to three because we have exactly three signal types to cluster. Our metric for classification accuracy is the percentage of true predictions returned by knn, based off the signal type labels we assign. We found that τ values between 0.1 – 0.9 classify signal types to the ~70% accuracy level, and we do not observe appreciable changes between τ values to the hundredths decimal point. We only have twenty labeled signals to work with at MDJ, so using a larger signal database (for a given station) could give us more robust statistics. Using either nonlinear alignment methods suggests that the explosion waveforms are separated from earthquake waveforms, but the collapse event may group with either the earthquake (DTW) or explosion (ESA) population. The results shown for MDJ do not dramatically change if the signal envelope is used, or if the R and T component waveforms are concatenated to Z.

We report which ground motion component, signal type, window length and frequency passband that best distinguishes explosion from non-explosion signals for our full set of regional stations in Table 1. The criterion for choosing a particular passband is an improvement in classification accuracy. We list how the LOO cross validation with knn performed for D_x, D_y and DTW_{dist} separately to see if any one distance is superior to another (Table 1). For stations less than 300 km from the source, knn classification using D_y performs comparably to DTW_{dist} and slightly better than D_x. Stations at greater distances (>300 km) from the source do not record waveforms with qualities that are sufficient for this type of analysis (i.e., SNR > 3). This may impact classification accuracy as it is essentially the same between all distance metrics at SEO2 (Table 1). Note also that the relative time window accordingly widens to accommodate larger P to L_g separation time. For the τ analysis at station MDJ, we attempted to find the best linear combination of D_x and D_y that improved classification accuracy, but ultimately found that D_y by itself is superior, which may not be the case for every dataset. Moreover, there is no reason to stick to a linear relationship between the phase and amplitude distance matrices; this assumption may be relaxed in future work. For most of the signals analyzed here, there is little improvement in accuracy between the signal waveforms compared to the envelope functions (for the frequency bands considered here), but this topic deserves further exploration.

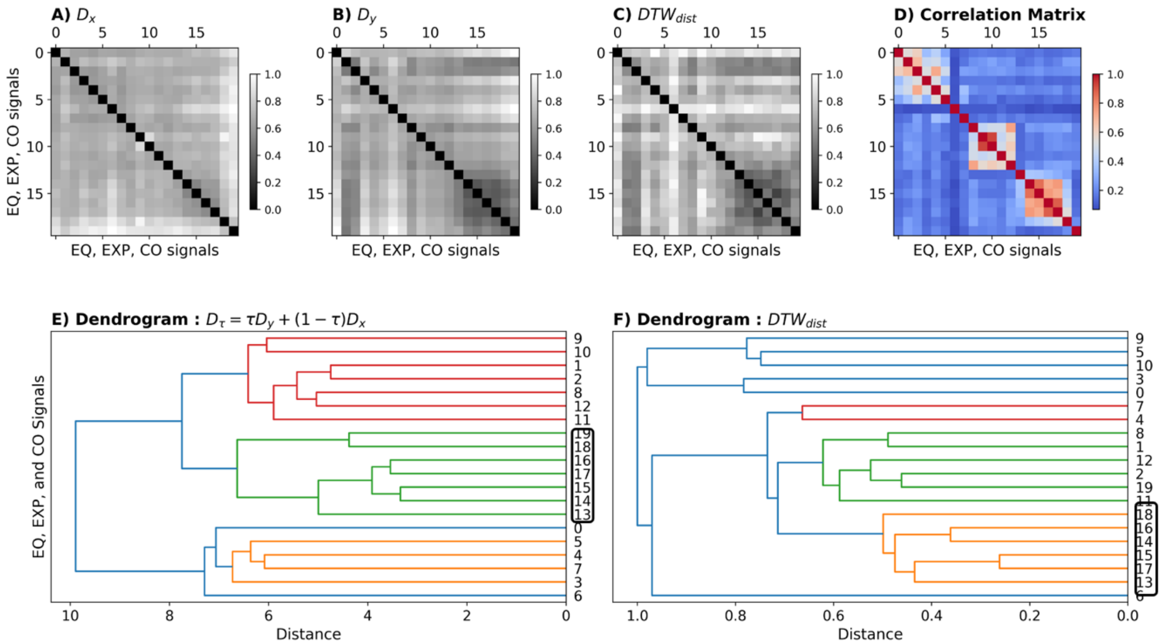

Figure 4. Cluster analysis at station MDJ. Indices along the axes in (A)-(D) are as follows: 0 – 12 (earthquake), 13 – 18 (explosion) and 19 (collapse). A) Phase distance, B) amplitude distance, C) DTW distance, and D) maximum cross-correlation coefficient between every earthquake, explosion and collapse signal pair. The diagonal of each symmetric distance matrix is zero or one. E) and F) show the dendrogram trees from hierarchical cluster analysis for ESA and DTW, respectively. In E), a value of 0.5 is used for the coefficient τ (Eq.5). The indices corresponding to explosions are enclosed by the black rectangle

Discussion

Method Sensitivity and Comparison

We conceptually showed how nonlinear warping distances can distinguish dissimilar signal types using synthetics, and when we applied advanced clustering on the actual data, we saw that modest classification accuracies can be achieved. This result may stem from complex wave propagation that is generally not captured when using a 1-D or laterally homogenous earth model but is certainly present in the real Earth. Differences between source types can be deduced from narrowband filters, as is commonly used in P_g/L_g ratio analyses (Pyle and Walter, 2021; Tibi et al., 2023). Similarly, the selection of an appropriate filtering passband, minimum SNR, and consequently, time window length was central to our analysis. For MDJ, we analyzed several frequency passbands to capture lower-frequency L_g (< 1Hz) or higher frequency P (> 2 Hz). All signal types from this dataset were present at MDJ, and our clustering approach is most accurate for this station. However, we acknowledge that this is a small, imbalanced dataset and future work should target a labeled database of diverse source types with varying SNR so that the DTW/ESA framework can be further assessed in comparison to neural network classifiers (e.g., Eggertsson et al., 2024; Maguire et al., 2024) or other discrimination approaches. Recently, focal depth discriminants have been developed at local-to-regional distances that use differential magnitudes or spectral amplitude ratios (i.e., R_g/S_g, P_g/S_g) between mine blasts and earthquakes (Koper et al., 2024). In this study, the depth was held constant in the synthetic experiment (1 km) and was 5-km and shallower for the DPRK dataset. There is opportunity to extend the nonlinear alignment framework for depth discrimination as well since focal depth differences can influence body and surface wave excitation (Zhang et al., 2002).

Optimal Signal Separation and Monitoring Implications

Previous studies have shown that for ESA, either amplitude or phase distance can perform better for a particular signal classification application (Tucker et al., 2014) and linear combinations of them can provide better results than using either one alone. Using MDJ as an example, we saw that D_y by itself and the joint combination of D_y and D_x had a greater classification accuracy than D_x (Table 1, Figure 4). Why might that be? It could be due to the higher relative P_n and P_g amplitudes on the explosion waveforms, which are present across a wide frequency band. Alternatively, it may be due to the complexity of phase information between these source types, which suggests phase-based metrics alone may not offer a simple interpretation. We are also interested is the relationship between cross-correlation coefficient and phase or amplitude distance, as well. We showed that a given distance matrix has an inverse relationship to the similarity matrix, consistent with our hypothesis that any two highly similar signals will have a smaller distance between them in phase or amplitude spaces (Figures 1 and 4). ESA could be adapted to assist empirical cross-correlation signal detection by extending the correlation range of templates to account for small differences in source mechanism or Green's function. One of the biggest shortcomings of standard correlation detectors is the curation of an optimal template library and appropriate detection statistic (Gibbons, 2022). We believe automatic event screening could leverage one (or more) signal distance spaces to address this issue.

Conclusion

We have shown that nonlinear alignment techniques such as DTW or ESA have potential to discriminate signal types, with special consideration to frequency content, time-window, and component analyzed. Low magnitude events may be difficult to classify due to their lower SNR when regional distance stations are used. The potential advantage of the discriminant method we presented here is that one can use the full waveform, increasing the available time bandwidth product. Future directions include examining the transportability of this discriminant method using a larger regional dataset, systematic evaluation of how monitoring distance, frequency passband, or how varying SNR influences results.

Data and Resources

To replicate our workflow, the *Computer Programs in Seismology* (CPS) software must be compiled (installation here: https://www.eas.slu.edu/eqc/eqccps.html). Earthquake, collapse, and explosion waveforms are freely accessible through the IRIS data web-service (last accessed on May 10, 2024). Maps are made using the PyGMT software (Uieda et al., 2023).

Declaration of Competing Interests

The authors acknowledge that there are no conflicts of interest recorded.

Acknowledgements

This Ground-based Nuclear Detonation Detection (GNDD) research was funded by the National Nuclear Security Administration, Defense Nuclear Nonproliferation Research and Development (NNSA DNN R&D). Sandia National Laboratories is a multimission laboratory managed and operated by National Technology & Engineering Solutions of Sandia, LLC, a wholly owned subsidiary of Honeywell International Inc., for the U.S. Department of Energy's National Nuclear Security Administration under Contract Number DE-NA0003525. ChatGPT, or any variation thereof, was not used to write any part of this manuscript. We thank Derek Tucker for discussions on the application of Elastic Shape Analysis and Bob Herrmann for assistance with CPS.

References

Alvizuri, C., and C. Tape (2018). Full moment tensor analysis of nuclear explosions in North Korea. *Seis. Res. Lett.*, 89(6), 2139–2151. https://doi.org/10.1785/0220180158.

Anderson, K. R. and J. E. Gaby (1983). Dynamic Waveform Matching. *Information Sciences*, 31, 221 – 242.

Ben-Menahem, A. and Singh, S.J. (198). Seismic Waves and Sources, Springer Verlag, New York, NY.

Chun, K-Y and P. G. Richards (2004). *Dongbei Broadband Network* [Data set]. International Federation of Digital Seismograph Networks. https://doi.org/10.7914/SN/5G_2004.

Eggertsson, G., Lund, B., Roth, M., and Schmidt, P. (2024). Earthquake or blast? Classification of local-distance seismic events in Sweden using fully connected neural networks, *Geophys. Jour. Int.*, 236, 1728 – 1742, doi.org/10.1093/gji/ggae018.

Ford, S. R., D. S. Dreger, and W. R. Walter (2009). Source Analysis of the Memorial Day explosion, Kimcaek, North Korea, *Geophys. Res. Lett.,* 36, L21304, doi:10.1029/2009GL040003.

Gibbons, S. J. (2022). The optimal correlation detector?, *Geophys. Jour. Int.*, 228, 355 – 365, doi.org/10.1093/gji/ggab344.

Hale, D. (2013). Dynamic warping of seismic images, *Geophys.*, 78(2), S105–S115.

Herrmann, R. B. (2013). Computer programs in seismology: An evolving tool for instruction and research, *Seism. Res. Lettr.* **84**, 1081-1088, doi:10.1785/0220110096.

Joshi, S.H., E. Klassen, A. Srivastava, I. H. Jermyn (2007). A novel representation for Riemannian analysis of elastic curves in Rn, *Proceedings of IEEE CVPR*. pp. 1–7.

Kumar, U., C. P. Legendre, L. Zhao, and B. F. Chao (2022). Dynamic time warping as an alternative to windowed cross correlation in seismological applications, *Seismological Research Letters*, 93(3), 1909–1921. doi: 10.1785/0220210288.

Kong, Q., R. Wang, W. R. Walter, M. Pyle, and B. Schmandt (2022). Combining Deep Learning With Physics Based Features in Explosion-Earthquake Discrimination, *Geophys. Res. Lett.*, 49, e2022GL098645. https://doi.org/10.1029/2022GL098645

Linville, L., K. Pankow, and T. Draelos, T. (2019). Deep learning models augment analyst decisions for event discrimination, Geophys. Res. Lett., 46, 3643–3651. https://doi.org/10.1029/2018GL081119.

Maguire, R., B. Schmandt, R. Wang, Q. Kong, and P. Sanchez (2024). Generalization of Deep-Learning Models for Classification of Local Distance Earthquakes and Explosions across Various Geologic Settings, *Seismol. Res. Lett*. XX, 1–10, doi: 10.1785/ 0220230267.

Mikesell, T. D., A. E. Malcolm, D. Yang and M. H. Haney (2015). A comparison of methods to estimate phase delays: numerical examples for coda wave interferometry, *Geophysical Journal International*, 202, 347 – 360, doi: 10.1093/gji/ggv138.

Müller, M. (2021). Fundamentals of music processing using Python and Jupyter notebooks, *Springer,* doi:10.1007/978-3-030-69808-9.

Myers, S. C., S. R. Ford, R. J. Mellors, S. Baker, and G. Ichinose (2018). Absolute locations of the North Korean nuclear tests based on differential seismic arrival times and InSAR. *Seismological Research Letters*, 89(6), 2049–2058. https://doi.org/10.1785/0220180123.

Pasyanos, M. E. and A. Chiang, (2022). Full moment tensor solutions of U.S. underground nuclear tests for event screening and yield estimation, *Bull. Seis. Soc. of Amer.*, 112, 538–552.

Pyle, M. L., and W. R. Walter (2021). Exploring the Effects of Emplacement Conditions on Explosion P/S Ratios across Local to Regional Distances, *Seismol. Res. Lett*. 93, 866–879, doi: 10.1785/0220210270.

Srivastava, A., E. Klassen, S. Joshi, and I. Jermyn (2011). Shape analysis of elastic curves in Euclidean spaces. *IEEE Transactions on Pattern Analysis and Machine Intelligence* 33 (7), 1415–1428.

Stevens, J. L. and S. M. Day (1985). The physical basis of mb: MS and variable frequency magnitude methods for earthquake/explosion discrimination. *Journal of Geophysical Research*, 90, 3009–3020.

Tan, J., and C. A. Langston (2022). Shape Dynamic Time Warping for Seismic Waveform Inversion, *Bulletin of the Seismological Society of America*, XX, 1–18, doi: 10.1785/0120220051.

Tibi, R. (2021). Discrimination of Seismic Events (2006– 2020) in North Korea Using P/Lg Amplitude Ratios from Regional Stations and a Bivariate Discriminant Function, *Seismol. Res. Lett.* 92, 2399–2409, doi: 10.1785/0220200432.

Tibi, R., N. Downey, and R. Brogan (2023). Testing and Design of Discriminants for Local Seismic Events Recorded during the Redmond Salt Mine Monitoring Experiment, *Bull. Seismol. Soc. Am.* 114, 906–923, doi: 10.1785/0120230193.

Tucker J. D., Wu, W., and Srivastava, A (2013). Generative models for functional data using and amplitude separation, *Comp. Stats. and Data Analysis* 61, 50 – 66, doi:10.1016/j.csda.2012.12.001.

Tucker, J. D., W. Wu, and A. Srivastava (2014). Analysis of signals under compositional noise with applications to SONAR data, *IEEE Journal of Oceanic Engineering*, vol 29, no. 2. pp 318-330.

Uieda, L., Tian, D., Leong, W. J., Schlitzer, W., Grund, M., Jones, M., et al. (2023). PyGMT: A Python interface for the Generic Mapping Tools. (v0.9.0) [Software]. Zenodo. https://doi.org/10.5281/zenodo.7772533.

Walter, W. R., D. A. Dodge, G. Ichinose, S. C. Myers, M. E. Pasyanos, and S. R. Ford (2018). Body-wave methods of distinguishing between explosions, collapses, and earthquakes: Application to recent events in North Korea, *Seismol. Res. Lett*. 89, 2131–2138.

Yuan, C., J. Bryan, and M. Denolle (2021). Numerical comparison of time-, frequency and wavelet-domain methods for coda wave interferometry, *Geophysical Journal International*, 226(2), 828–846, doi: 10.1093/ GJI/GGAB1.

Zhang, J., T. Lay, J. Zaslow, and W. R. Walter (2002). Source effects on regional seismic discriminant measurements, *Bull. Seismol. Soc. Am*. 92, 2926–2945.

Tables

Table 1: Hierarchical Clustering Results for Regional Seismic Stations. Note that due to data availability issues or low SNR, not all events are included at a particular station.

Component(s)	Signal Type	Events Included	Source Receiver Distance (km)	Window Length (sec)	Filter band (Hz)	% Accuracy (Dx)	% Accuracy (Dy)	% Accuracy (DTWdist)
BHN	Waveform	EQ1, EQ2, EQ7, NK5, NK6, CO	344.1	100	0.8 – 8.0	33	45	40
BHZ	Waveform	EQ1, EQ2, EQ3, EQ4, EQ5, EQ6, EQ7, EQ8, EQ9, EQ10, EQ11, EQ12, EQ13, NK1, NK2, NK3, NK4, NK5, NK6, CO	371.0	100	0.5 – 5.0	65	90	90
BHN	Waveform	EQ1, EQ2, EQ3, EQ9, EQ10, EQ11	461.8	120	0.8 – 6.0	67	67	67

Station	Network
SEHB	KS
MDJ	IC
MDJ	KS
SEO2	KS